Journal Pre-proof

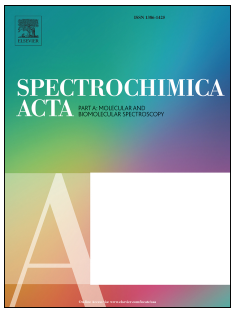

Effect of carbamylation on the molecular recognition action of amino benzothiazole by carrier protein

Hua-xin Zhang, Qing-hua Xia, Dan Zhou

PII: S1386-1425(19)30985-0

DOI: https://doi.org/10.1016/j.saa.2019.117595

Reference: SAA 117595

To appear in: *Spectrochimica Acta Part A: Molecular and Biomolecular Spectroscopy*

Received Date: 24 July 2019

Revised Date: 12 September 2019

Accepted Date: 2 October 2019

Please cite this article as: H.-x. Zhang, Q.-h. Xia, D. Zhou, Effect of carbamylation on the molecular recognition action of amino benzothiazole by carrier protein, *Spectrochimica Acta Part A: Molecular and Biomolecular Spectroscopy* (2019), doi: https://doi.org/10.1016/j.saa.2019.117595.

Graphical abstract

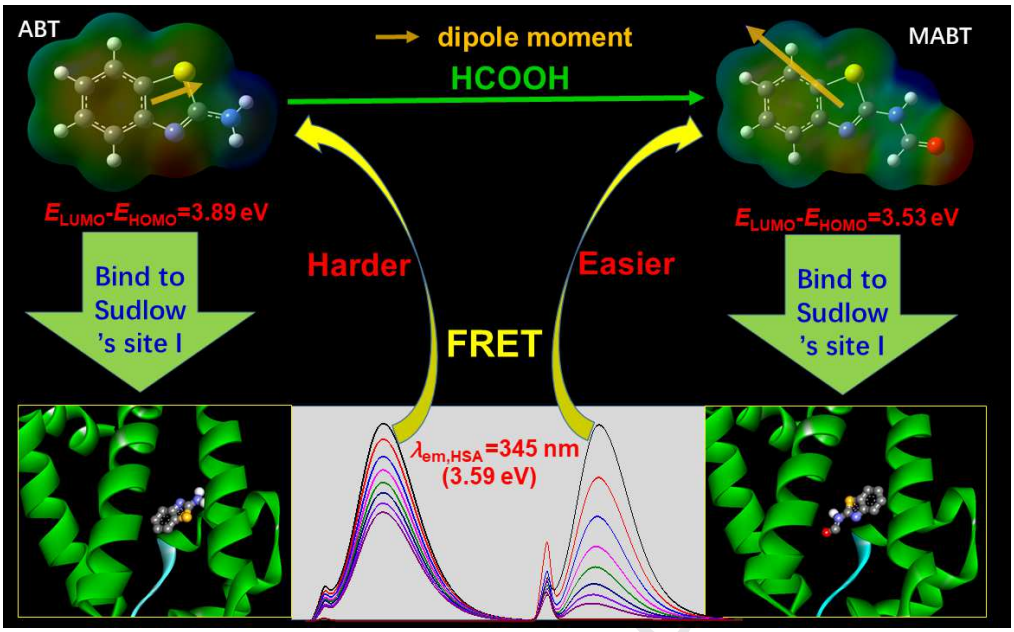

The hydrophobic heterocyclic scaffold of benzothiazole guided ABT and MABT to Sudlow's site I in the subdomain IIA of HSA, while the carbamylation of ABT on position 2 resulted in the opposite molecular orientation and significantly increased energy reception efficiency, which were reasonably explained by the alterations of dipole moment and energy gap between HOMO and LUMO.

Effect of carbamylation on the molecular recognition action of amino benzothiazole by carrier protein

Hua-xin Zhang[a, b, *], Qing-hua Xia[a], Dan Zhou[a, *]

[a]Ministry-of-Education Key Laboratory for the Synthesis and Application of Organic Functional Molecules, Hubei University, Wuhan 430062, P. R. China

[b]Hubei Key Laboratory of Drug Synthesis and Optimization, Jingchu University of Technology, Jingmen 448000, P. R. China

*Corresponding authors.
Tel.: +8618986973258
*E-mail addres*s: h.x.zhang@yeah.net (H. X. Zhang), d.zhou@hubu.edu.cn (D. Zhou)

Abstract:

Increasing benzothiazole derivatives containing amino or N-acyl structures in position 2 have been largely developed as pesticides and medicines. However, the structure-function relationship of 2-substituted benzothiazole derivatives has seldom been illustrated from the perspective of their albumin-binding nature. Herein, to probe the influence of carbamylation on the albumin-binding nature of benzothiazole derivatives, formyl group was introduced to the amine group of 2-amino benzothiazole (ABT) to yield a novel modified ABT (MABT). Their protein-binding properties were systematically deciphered by spectroscopy, molecular modeling and density functional theory (DFT) calculations. The interaction mechanisms, recognition thermodynamics and binding geometry were investigated and compared. The structural alteration of human serum albumin was explored using synchronous fluorescence emission and circular dichroism spectrum technologies. Based on experimental results, the structures of protein complex with MABT and ABT were revealed by molecular docking method. The differences in energy transfer efficiency and molecular orientation of ABT and MABT in new complexes were tentatively explained by DFT calculations. The work was expected to help to understand the impact of different substituents on the bioactivity of benzothiazole derivatives and guide for structural designs of new compounds.

Keywords: Benzothiazole derivative; Fluorescence probe; Molecular modeling; Thermodynamics; DFT

1. Introduction

The biological action of an active compound is highly dependent on its binding tendency to plasma proteins since many key physiological processes of exogenous molecules are closely related to their protein-binding ratio, such as transportation, distribution and clearance [1-3]. The nature of plasma-binding has become one of the essential items when evaluating a new compound which is going to be applied in vivo [4].

Benzothiazole, chemically referred to as 1,3-benzothiazole, is an aromatic heterocyclic compound, whose activity is obviously superior to other heterocyclic because of the introduction of sulfur atoms. The nine atoms in this heterocyclic scaffold are coplanar, which provides its derivative a steady chemical structure that allows more applications. When substituents are attached, this molecule becomes especially active in biology, which makes benzothiazole derivatives gained great attention and widely used in pesticide, medicine and other fields [5].

The type and the position of substituent group are two main factors that influence the physiological and biological activities of benzothiazole derivatives. Since this heterocyclic stem nucleus is electron-withdrawing group, electron-donating substituent should be favorable for increasing biological activity. On the other hand, a large number of experiments show that 2-substituted benzothiazole has higher activity. Considering these two points, 2-amino benzothiazole (ABT) was selected as a target ligand. To inspect the influence of the electron-donating ability of substituent group on the protein-binding properties of benzothiazole derivatives, a novel modified ABT, N-1, 3-benzothiazol-2-ylformamide (MABT) was synthesized for comparison.

The scaffolds of ABT and MABT exist in plenty of commercial products such as riluzole (an amyotrophic lateral sclerosis drug), frentizole (an antiviral drug and immunosuppressant), benzthiazuron and methabenzthiazuron (pesticides) (Fig. 1) and there are still a large number of substituted active compounds being researched as candidates for pesticides and drugs [6]. So, the present study is of considerable value.

The task of present paper was: (1) to synthesize MABT from ABT by formylation reaction of amine group; (2) to investigate the interaction of HSA with ABT and MABT respectively, including interaction mechanisms, recognition thermodynamics and binding geometry, binding power, and the structure of protein-ligand complex; (3) to analyze the difference in serum-binding characteristics between ABT and MABT, and to explain the reasons. This study was expected to help to understand the action mechanism of benzothiazole derivatives with different substituents and guide for their structural designs.

2. Experimental

2.1. Chemicals

HSA，warfarin and tris(hydroxymethyl)aminomethane (Tris) were supplied by Sigma-Aldrich Chemical Co. (Milwaukee, USA). Ibuprofen and KCl were purchased from Roche Diagnostics (Mannheim, Germany). 2-amino benzothiazole (ABT) was purchased from Macklin Inc. (Shanghai, China) and N-1, 3-benzothiazol-2-ylformamide (MABT) was synthesized in our laboratory.

The buffer of pH 7.40 was prepared by mixing 0.05 M Tris aqueous and 0.15 M HCl aqueous at proper ratio and KCl (0.5 M) was added to simulate physiological condition. The working solution of ABT (0.5 mM), MABT (0.5 mM), ibuprofen (10 mM) and warfarin (10 mM) were dissolved by

ethanol. HSA solution (50 μM) was dissolved by buffer. 2 mL of 50 μM HSA solution and different volumes of ABT or MABT were mixed in a battery of 10 mL colorimetric tubes and diluted to scale lines with buffer. The mixtures were kept at specific temperature for 0.5 h before spectroscopic determination.

2.2. Instruments

All fluorescence was measured on a Hitachi F-4600 fluorescence spectrophotometer. The temperature was maintained by a thermostatic circulator bath. A Jasco J-810 Spectropolarimeter, a Purkinje TU-1901 spectrophotometer, a Testo 206-pH2 pH-meter and a Mettler-Toledo Excellence plus electronic analytic balance were employed to record CD spectra, UV-vis spectra, pH values and weights, respectively.

2.3. Inner filter effect correction

The data were corrected by equation 1, as described in literatures [7, 8]:

$$F_{cor} = F_{obs} 10^{\frac{1}{2}(Aex+Aem)} \quad (1)$$

2.4. Molecular docking

Molecular modeling for ABT-HSA and MABT-HSA complexes was performed by the famous docking software AutoDock 4 [9]. The concrete procedures were based on literature [10] as experiments had revealed the definite binding site of present ligands.

2.5. DFT study

All computation results were given by ORCA (Version 4.0.1) [11]. The researches were done in the gas phase, and M06-L functional with 6-311G(d) basis set was employed [12], which was thought to be one of the functionals with small errors [13]. The electrostatic potential was drawn on ABT and MABT molecule and visualized by VMD (Version 1.9.3) program [14].

2.6. Synthesis of MABT

MABT was synthesized from ABT by formylation reaction of amine group (Fig. 2). Formic acid (88%) was dried by anhydrous magnesium sulfate and filtered. 2.5 g of dried formic acid (54 mmol) and 7.1 g of diacetyl oxide (69 mmol) was mixed and refluxed for 3h. Then, the temperature was kept lower than 40 □1 and 3 g of ABT (8.7mmol) were gradually added to the mixed acid anhydride. Afterwards, 15 mL of $H_5C_2OC_2H_5$ was added and stirred for another 22 h. The residues were filtered and washed by diethyl ether for several times, affording the white solid product (in a yield of 42.0%).

3. Results and Discussions

3.1. The emission spectra

Aromatic amino acid residues in HSA make this protein a fluorophore, which can give intensive fluorescence near 345 nm when excited by ultraviolet radiation. Fig. 3 recorded the fluorescence emission spectra of ABT, MABT, HSA and their mixed systems between 280 nm and 480 nm.

As we could see in Fig. 3, even at their highest concentration in systems, both ABT and MABT gave little fluorescence at 345nm when excited by 285 nm. It suggested ABT or MABT made no contribution to the emission intensity of HSA, which ensured the reliability of the data. When HSA was fixed at 10 μM, the emission intensity decreased with increasing amount of ABT (Fig.3 A) and MABT (Fig.3 B), which was usually referred as fluorescence quenching [15, 16]. MABT showed obviously stronger quenching ability than ABT in the same concentrations, which implied that the energy transfer efficiency between protein and ligand significantly enhanced when the amine group

was replaced by the acylated amine group.

3.2. The quenching mechanism

Fluorescence quenching contains dynamic and static mechanism [17]. These two types can be judged by the fluorescence lifetime of phosphor at excited state, the relationship between quenching constant and temperature or the ultraviolet spectra of interaction systems [18, 19]. In our experiments, the quenching spectra were recorded at 310K, 304K, 298K and 292K, respectively. The corrected emission intensity data were plotted by Stern-Volmer equation [20]:

$$\frac{F_0}{F} = 1 + K_{SV}[Q] \qquad (2)$$

Assuming their quenching belonged to dynamic mechanism, the slopes of regression equation (i.e. Stern-Volmer constant, K_{SV}) should represent dynamic quenching constants and it should increase when temperature rises [21]. But the Stern-Volmer constants of ABT-HSA systems (Fig.4A) decreased from 5.381×10^3 L·mol^{-1} at 292 K to 4.437×10^3 L·mol^{-1} at 310 K, and MABT-HSA systems (Fig.4B) from 5.186×10^5 L·mol^{-1} at 292 K to 4.436×10^5 L·mol^{-1} at 310 K. The dynamic quenching constants we detected were inversely correlated with temperature. It was untenable because higher temperature would always promote diffusion. Therefore, our previous assumption of dynamic quenching could be ruled out.

To confirm the quenching mechanism, ultraviolet absorption of ABT, MABT, HSA and their mixed systems were recorded (Fig. 5). From Fig. 5 we could see, the absorbance of HSA-ligand systems around 220 nm (blue curves) was much lower than the superposition (light violet curves) of the separated absorbance of HSA (black curves) and ligands (red curves), which indicated that HSA had formed new complex with both ABT and MABT at ground state [22]. Considering the results of quenching constants and ultraviolet spectra, the quenching process between ABT/MABT and HSA

could be identified as static mechanism.

3.3. Binding thermodynamics

Static quenching means new complex formation. The observed binding constant (K_b) and binding site number (n) could be calculated by the logarithm equation described in literature [23]:

$$\log(\frac{F_0 - F}{F}) = \log K_b + n\log[Q] \qquad (3)$$

The plots and regression equations were presented in Fig. 6. Thermodynamic parameters are important in evaluating the affinity between ABT/MABT and HSA [24]. The ΔH^θ and ΔS^θ of an isobaric process can be calculated by the indefinite integral form of Van't Hoff equation (Fig. 7):

$$\ln K = \frac{-\Delta H^\theta}{RT} + \frac{\Delta S^\theta}{R} \qquad (4)$$

And ΔG^θ can be calculated by its definition:

$$\Delta G^\theta = \Delta H^\theta - T\cdot\Delta S^\theta \qquad (5)$$

The considerable value of binding constants in Table 1 means both ABT and MABT can bind effectively with HSA. The order of binding constants between HSA and MABT (10^7) is one thousand times bigger than ABT (10^4), indicating the stability of MABT-HSA complex is higher than ABT-HSA. The negative ΔG^θ and positive ΔS^θ suggests the interactions between ABT/MABT and HSA are spontaneous and entropy-driven process. But the protein-binding tendency of MABT is much greater. The most obvious distinction between ABT and MABT is their enthalpy changes (ΔH^θ) when binding to HSA. ABT-HSA interaction is an exothermic process while MABT-HSA interaction is an endothermic one, which should be considered when designing pesticide or drug molecules based on benzothiazole scaffold.

3.4. The binding powers

According to the thermodynamic rules reported by Ross [25], it could be speculated that the main powers that stabilized the structures of ABT-HSA and MABT-HSA complex was electrostatic forces and hydrophobic interactions, respectively.

3.5. The conformation investigation

Synchronous fluorescence emission (SFE) techniques has been widely applied to detect the nature of amino acid residues in protein [26]. The shift of maximum emission wavelength in synchronous spectra reflects the changes in polarity around the chromophore: a red shift means an increase in the polarity while a blue shift denotes an increase in hydrophobicity [23]. Based on these rules, we could infer that the binding of ABT had led to increases in polarity around both tryptophan residue and tyrosine residue in HSA, as the maximum emission wavelength of both tryptophan and tyrosine moved to long wavelength direction (Fig. 8 A and B). The binding of MABT to HSA made no obvious impact on the microenvironment of tryptophan (Fig. 8 C) but the polarity around tyrosine strikingly increased (Fig. 8 D).

To quantitatively detect the influence of ABT/MABT binding, circular dichroism (CD) spectroscopy is employed [27]. The data of CD spectra were converted to mean residue ellipticity (Fig. 9) and used to calculate the fine structures (Table 2).

It could be found in Table 2 that ABT and MABT had altered the contents of fine structures. The total α-helix structure reduced by 2.9% (59.9% to 57.0%) and 8.5% (59.9% to 51.4%) after ABT and MABT were added, respectively. The total β-strand structure increased by 1.2% (5.8% to 7.0%) and 4.2% (5.8% to 10.0%), respectively. Under the same conditions, MABT brought more significant changes in total α-helix and β-strand structures. Similar cases could also be found in the

content of β-turns and irregular structure. These data demonstrated MABT would bring greater influence on the secondary structure of proteins than ABT. It implied that pesticides or drugs containing ABT and MABT scaffolds might present different activity or side effect.

3.6. Site-selective binding on HSA

To find out the binding site of ABT and MABT, warfarin and ibuprofen were used as molecular probes for Sudlow's site I and site II [28, 29], respectively. The spectra data (Fig. 10) were fitted by equation 3 (Fig. 11) to calculate the new binding constants. As expected, the value of K_b decreased after molecular probes were added, but in strikingly different levels. For both ABT and MABT, the influence of warfarin was obviously stronger than ibuprofen (insets of Fig. 11), which implied the warfarin had occupied the site of ABT and MABT. So, the primary site for ABT and MABT was Site I. It might be the heterocyclic scaffold of benzothiazole that guided the compound to specified binding site.

3.7. Molecular docking

The 3D crystallographic structure reported by He and Cater [30, 31] shows that HSA is a heart-shaped molecule consisting of 585 amino acid residues. Each of its three domain compromises ten helices which are ascribed to two subdomains. The first six helices are regarded as subdomain A and the last four as subdomain B.

Since the site markers experiments have revealed the binding site of ABT and MABT locates in Sudlow's site I, the grid centers were set at 32.895, 13.107 and 7.466. The optimal docking results showed that ABT and MABT bound almost the same location in site I in the subdomain IIA (Fig. 12), based on which we thought it was amine group and heterocyclic scaffold of benzothiazole that guided ABT and MABT into the binding location . Though binding in the same location, the

molecular orientations of ABT and MABT were almost precisely opposite in new complexes, as shown in Fig. 13.

In Fig. 14, the residues close to ABT and MABT (within 3.5Å) were displayed, which showed ABT and MABT molecule were surrounded by different residues in subdomain IIA. The residues that directly interact with ABT mainly distributed on the amino terminal, leaving the left semi-sphere (benzene terminal) uncovered, as shown in Fig. 14A. It looked like some attractive force had pulled ABT molecule to the right side and we speculated two gravitations might be responsible for it. Firstly, the only one hydrophilic residue (SER287) within 3.5Å was located in the amino terminal of ABT molecule. Secondly, the carboxyl oxygen of ARG257 formed two hydrogen bonds (H-bonds) with the amine group of ABT. The existence of H-bonds was complied with the conclusion on the binding power between ABT and HSA in *Section 3.4.*

On the other hand, MABT was entirely enclosed by a closed pocket made up of LUE219, ARG222, PHE223, LEU238, VAL241, ARG257, LEU260, ALA261, ILE264, SER287, ILE290 and ALA291 (Fig. 14B). Most of these residues are hydrophobic, indicating the primary power fixing MABT was hydrophobic interactions, which was also in accordance with the result of thermodynamic discussion.

3.8. DFT calculations

In order to understand the difference in protein-binding characteristics of benzothiazole derivatives when amine group on position 2 was substituted by formamide group, DFT calculations were performed according to the method mentioned in experimental section. The electrostatic potential and the dipole moments of ABT and MABT molecules were presented in Fig. 15, where we could find that the dipole moments of two ligands were almost in opposite direction (blue

arrows in Fig. 15). It implied that electrostatic force existed not only in ABT-HSA complex as the primary power, but also in MABT-HSA complex as an auxiliary power that could not be ignored. Then the opposite orientation of ABT and MABT in protein-ligand complexes described in molecular docking study could be easily understood.

Another significant difference between HSA-ABT and HSA-MABT systems revealed by the results of fluorescence detection was the energy transfer efficiency. To analyze why HSA possessed obviously higher energy transfer efficiency to MABT than to ABT, the frontier molecular orbits of ABT and MABT were calculated and compared. According to the frontier molecular orbital theory, the electron transition from HOMO to LUMO is most easily to happen under external stimulus. The energy gap between HOMO and LUMO ($\Delta E = E_{LUMO}-E_{HOMO}$) of the ABT and MABT molecules were employed to analyze their efficiency of energy reception. The HOMO and the LUMO of ABT and MABT molecules in combination with their energy levels were listed contrastively in Table 3.

We could find in Table 3 that the energy levels of both HOMO and LUMO reduced when the amine group of ABT was substituted by formamide group, which suggested that the stability of MABT was superior to that of ABT. The energy gap (ΔE) of the ABT and MABT molecules were calculated to be 3.89 eV and 3.53 eV, respectively. The maximum fluorescence emission wavelength of HSA (energy donor) was 345 nm (Fig. 3), whose energy corresponded to 3.59 eV. It was obvious that the energy gap ($E_{LUMO}-E_{HOMO}$) of the ABT matched better with the energy of donor, which meant, compared to ABT, the valence electron of MABT was more easily to accept the energy and jump to unoccupied molecular orbital with higher energy levels. The theoretical reasoning based on structural calculation reasonably accounted for the experimental facts that MABT quenched the characteristic fluorescence of HSA much more effectively than ABT in the

same concentrations

4. Conclusions

In present paper, MABT was synthesized from ABT by formylation reaction of amine group. Then the protein-binding characteristics of ABT and MABT were systematically determined and compared. The results showed that both ABT and MABT could bind with HSA in vitro. The orders of equilibrium constants for MABT and ABT were 10^7 and 10^4 $L \cdot mol^{-1}$, respectively, indicating a higher energy transfer efficiency in HSA-MABT systems than HSA-ABT systems. Their interactions with HSA were entropy-driven ($\Delta S^{\theta}<0$) as well as spontaneous ($\Delta G^{\theta}<0$) processes, but with different heat effects (exothermic for ABT but endothermic for MABT). The primary power that stabilized the structures of ABT-HSA and MABT-HSA complex was electrostatic force and hydrophobic interaction, respectively. Compared to ABT, MABT caused greater influence on HSA's fine structure under the same conditions. Site marker competitive experiments suggested both ABT and MABT bound to Sudlow's site I. The optimal conformation presented the interaction details, which also rationally interpreted the conclusions drawn from spectral and thermodynamic studies. The energy gap between HOMO and LUMO of ABT and MABT molecules explained their different energy reception efficiency from HSA, and dipole moments were responsible for their opposite molecular orientation in new complex. Therefore, the hydrophobic heterocyclic scaffold of benzothiazole derivatives may determine their binding sites in protein, while the substitutes in position 2 will greatly affect the energy transfer efficiency, binding affinity, binding power and thermodynamics through altering the charge distribution of whole molecule.

Acknowledgements

We acknowledged the support of National Natural Science Foundation of China (21571055, 21673069) and Research Foundation of Education Bureau of Hubei Province (B2018240).

References

[1] P.R. Patlolla, N. Desai, S. Gupta, B. Datta, Interaction of a dimeric carbocyanine dye aggregate with bovine serum albumin in non-aggregated and aggregated forms, Spectrochim. Acta A 209 (2019) 256-263.

[2] F. Shiri, M. Rahimi-Nasrabadi, F. Ahmadi, H. Ehrlich, Multispectroscopic and molecular modeling studies on the interaction of copper-ibuprofenate complex with bovine serum albumin (BSA), Spectrochim. Acta A 203 (2018) 510-521.

[3] A. Kumar, M. Ali, R.S. Ningthoujam, P. Gaikwad, M. Kumar, B.B. Nath, B.N. Pandey, The interaction of actinide and lanthanide ions with hemoglobin and its relevance to human and environmental toxicology, J. Hazard. Mater. 307 (2016) 281-293.

[4] A.R. Timerbaev, C.G. Hartinger, S.S. Aleksenko, B.K. Keppler, Interactions of Antitumor Metallodrugs with Serum Proteins: Advances in Characterization Using Modern Analytical Methodology, Chem. Rev. 106 (2006) 2224-2248.

[5] D. Mene, M. Kale, Exploration of different methodologies for synthesizing biologically important benzothiazoles: an overview, Curr. Org. Synth. 13 (2016) 41-57.

[6] P. Chander Sharma, K. Kumar Bansal, A. Deep, M. Pathak, Benzothiazole Derivatives as Potential Anti-Infective

Agents, Curr. Top. Med. Chem. 17 (2017) 208-237.

[7] R.A. Leese, E.L. Wehry, Corrections for inner-filter effects in fluorescence quenching measurements via right-angle and front-surface illumination, Anal. Chem. 50 (1978) 1193-1197.

[8] M. Makarska-Bialokoz, A. Lipke, Study of the binding interactions between uric acid and bovine serum albumin using multiple spectroscopic techniques, J. Mol. Liq. 276 (2019) 595-604.

[9] G.M. Morris, R. Huey, W. Lindstrom, M.F. Sanner, R.K. Belew, D.S. Goodsell, A.J. Olson, AutoDock4 and AutoDockTools4: Automated docking with selective receptor flexibility, J. Comput. Chem. 30 (2009) 2785-2791.

[10] H.-x. Zhang, D. Zhou, Q.-h. Xia, Study on the molecular recognition action of lamivudine by human serum albumin, J. Mol. Recognit. (2018) e2705.

[11] F. Neese, The ORCA program system, Wiley Interdisciplinary Reviews: Computational Molecular Science 2 (2012) 73-78.

[12] Y. Zhao, D.G. Truhlar, A new local density functional for main-group thermochemistry, transition metal bonding, thermochemical kinetics, and noncovalent interactions, J. Chem. Phys. 125 (2006) 194101.

[13] D. Jacquemin, B. Mennucci, C. Adamo, Excited-state calculations with TD-DFT: from benchmarks to simulations in complex environments, Phys. Chem. Chem. Phys. 13 (2011) 16987-16998.

[14] W. Humphrey, A. Dalke, K. Schulten, VMD: visual molecular dynamics, J. Mol. Graph. 14 (1996) 33-38.

[15] J.R. Lakowicz, Principles of Fluorescence Spectroscopy, 3rd ed., Springer, New York 2006.

[16] M. Donmez, M.D. Yilmaz, B. Kilbas, Fluorescent detection of dipicolinic acid as a biomarker of bacterial spores using lanthanide-chelated gold nanoparticles, J. Hazard. Mater. 324 (2017) 593-598.

[17] M.S.J. Khan, Y.-W. Wang, M.O. Senge, Y. Peng, Sensitive fluorescence on-off probes for the fast detection of a chemical warfare agent mimic, J. Hazard. Mater. 342 (2018) 10-19.

[18] Y.J. Hu, Y. Ou-Yang, C.M. Dai, Y. Liu, X.H. Xiao, Site-Selective Binding of Human Serum Albumin by Palmatine:

Spectroscopic Approach, Biomacromolecules 11 (2010) 106-112.

[19] R. Yan, L. Lai, Z.-Q. Xu, F.-L. Jiang, Y. Liu, Thermodynamics of the Interactions between Quantum Dots and Proteins, Acta Phys. -Chim. Sin. 33 (2017) 2377-2387.

[20] A. Shamsi, M. Al Shahwan, S. Ahamad, M.I. Hassan, F. Ahmad, A. Islam, Spectroscopic, calorimetric and molecular docking insight into the interaction of Alzheimer's drug donepezil with human transferrin: implications of Alzheimer's drug, J. Biomol. Struct. Dyn. (2019) 1-9.

[21] H.-x. Zhang, E. Liu, D. Zhou, Q.-h. Xia, Structural and Thermodynamic Investigation into the Protein-Binding Properties of a Natural Product Crytotanshinone, J. Solution Chem. 47 (2018) 2068-2081.

[22] M. Makarska-Bialokoz, Analysis of the binding interaction in uric acid - Human hemoglobin system by spectroscopic techniques, Spectrochim. Acta A 178 (2017) 47-54.

[23] H.-x. Zhang, H.-x. Xiong, L.-w. Li, Investigation on the protein-binding properties of icotinib by spectroscopic and molecular modeling method, Spectrochim. Acta A 161 (2016) 88-94.

[24] Z.-Q. Xu, Q.-Q. Yang, J.-Y. Lan, J.-Q. Zhang, W. Peng, J.-C. Jin, F.-L. Jiang, Y. Liu, Interactions between carbon nanodots with human serum albumin and γ-globulins: The effects on the transportation function, J. Hazard. Mater. 301 (2016) 242-249.

[25] P.D. Ross, S. Subramanian, Thermodynamics of protein association reactions: forces contributing to stability, Biochemistry 20 (1981) 3096-3102.

[26] F.-l. Cui, L.-x. Qin, F. Li, H.-x. Luo, Synchronous fluorescence determination and molecular modeling of 5-Aminosalicylic acid (5-ASA) interacted with human serum albumin, J. Mol. Model. 14 (2008) 1111-1117.

[27] Y.-Z. Zhang, B. Zhou, X.-P. Zhang, P. Huang, C.-H. Li, Y. Liu, Interaction of malachite green with bovine serum albumin: Determination of the binding mechanism and binding site by spectroscopic methods, J. Hazard. Mater. 163 (2009) 1345-1352.

[28] G. Sudlow, D.J. Birkett, D.N. Wade, Further Characterization of Specific Drug Binding Sites on Human Serum Albumin, Mol. Pharmacol. 12 (1976) 1052-1061.

[29] A. Shamsi, A. Ahmed, B. Bano, Probing the interaction of anticancer drug temsirolimus with human serum albumin: molecular docking and spectroscopic insight, J. Biomol. Struct. Dyn. 36 (2018) 1479-1489.

[30] X.M. He, D.C. Carter, Atomic structure and chemistry of human serum albumin, Nature 358 (1992) 209-215.

[31] D.C. Carter, X.M. He, S.H. Munson, P.D. Twigg, K.M. Gernert, M.B. Broom, T.Y. Miller, Three-dimensional structure of human serum albumin, Science 244 (1989) 1195-1198.

361 **Table 1** Physical and chemical parameters for ABT-HSA and MABT-HSA interaction

Ligands	T(K)	K_b ($L \cdot mol^{-1}$)	n	ΔH^θ ($kJ \cdot mol^{-1}$)	ΔS^θ ($J \cdot mol^{-1} \cdot K^{-1}$)	ΔG^θ ($kJ \cdot mol^{-1}$)
ABT	292	1.873×10^4	1.139	-9.102	50.62	-23.88
	298	1.743×10^4	1.142			-24.19
	304	1.587×10^4	1.139			-24.49
	310	1.518×10^4	1.138			-24.80
MABT	292	1.840×10^7	1.671	2.899	149.0	-40.62
	298	1.895×10^7	1.681			-41.52
	304	1.929×10^7	1.694			-42.41
	310	1.976×10^7	1.698			-43.30

362

363

364 **Table 2** Alterations of fine structures of HSA

System	Regular α-helix (%)	Distorted α-helix (%)	Regular β-strand (%)	Distorted β-strand (%)	β-turns (%)	Unordered structure (%)
HSA	40.2	19.7	2.8	3.0	12.8	20.9
HSA-ABT	37.5	19.5	3.4	3.6	14.5	21.3
HSA-MABT	32.1	19.3	5.0	5.0	19.7	25.8

365

366

367 **Table 3** Frontier molecular orbital of ABT and MABT molecules.

Molecule	HOMO	E_{HOMO}/eV	LUMO	E_{LUMO}/eV	ΔE/eV
ABT	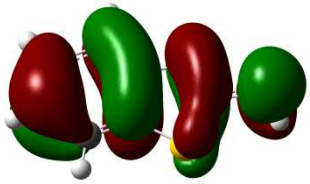	-5.24	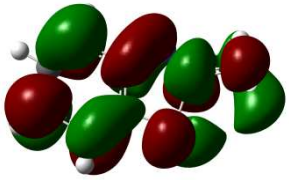	-1.35	3.89
MABT	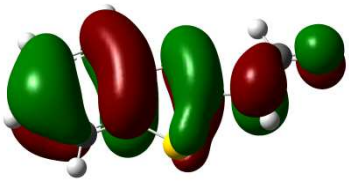	-5.82	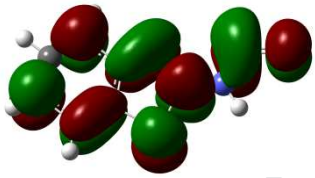	-2.29	3.53

368

369

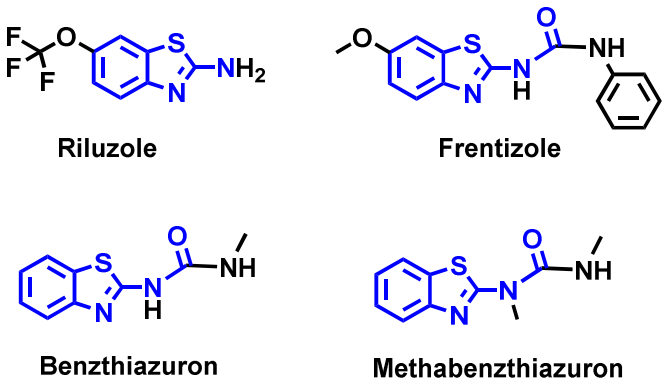

Fig. 1. Some commercial products containing the scaffold of ABT or MABT.

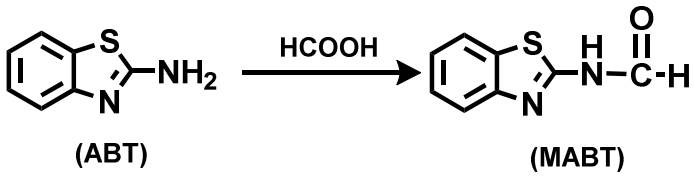

(ABT) (MABT)

Fig. 2. Synthetic route to MABT.

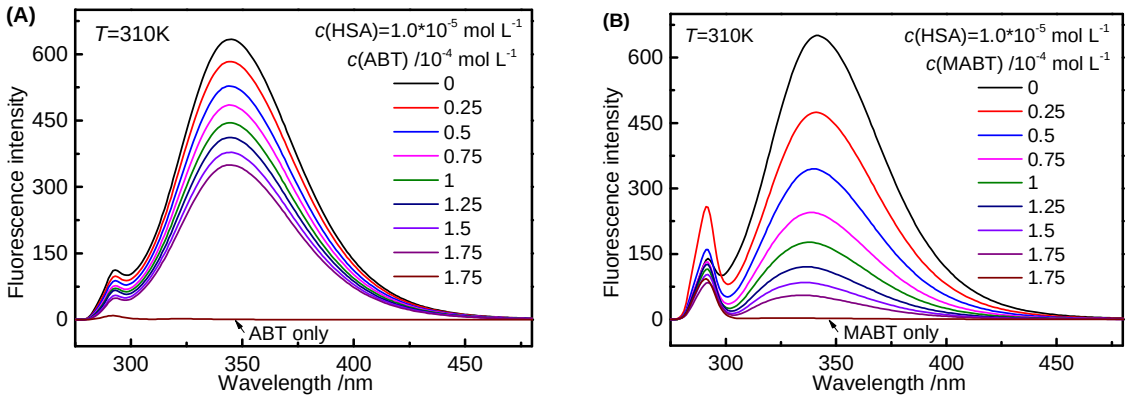

Fig. 3. Influence of ABT (A) and MABT (B) on the emission of HSA.

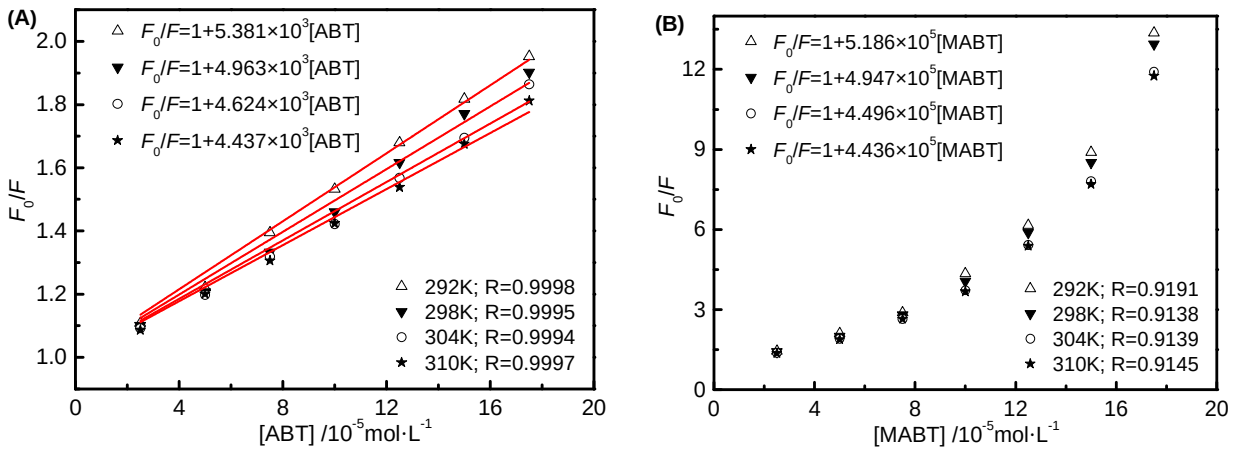

Fig. 4. Stern-Volmer plots of ABT-HSA systems (A) and MABT-HSA systems (B).

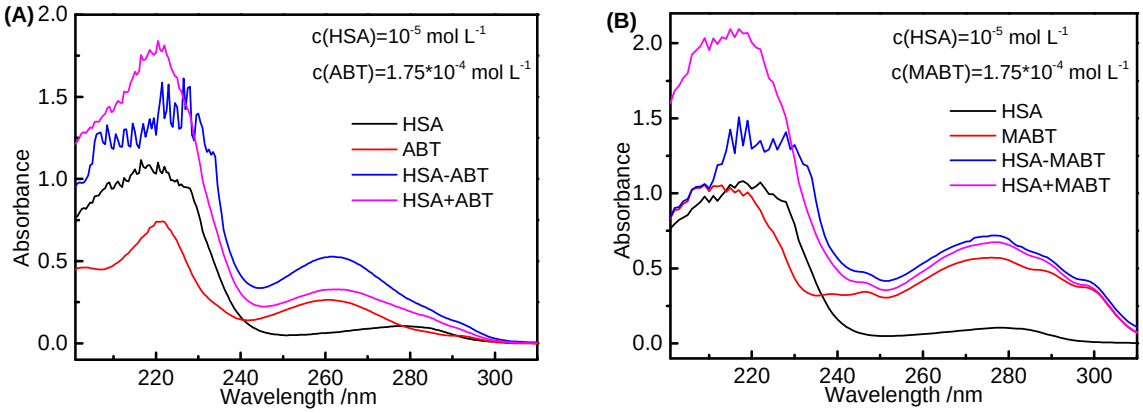

382

383 **Fig. 5.** Ultraviolet spectra of ABT-HSA systems (A) and MABT-HSA systems (B).

384

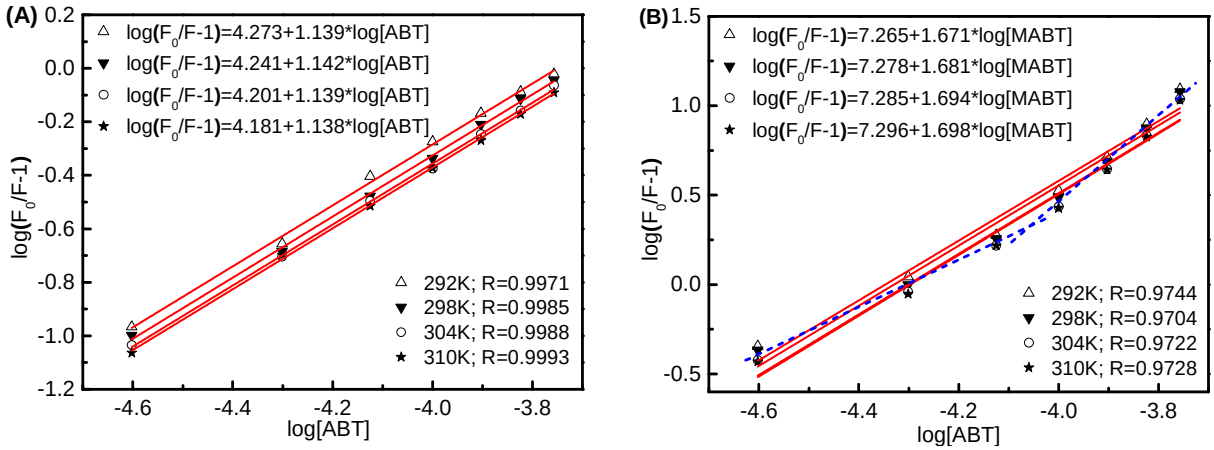

385

386 **Fig. 6.** Binding equilibriums of ABT-HSA systems (A) and MABT-HSA systems (B).

387

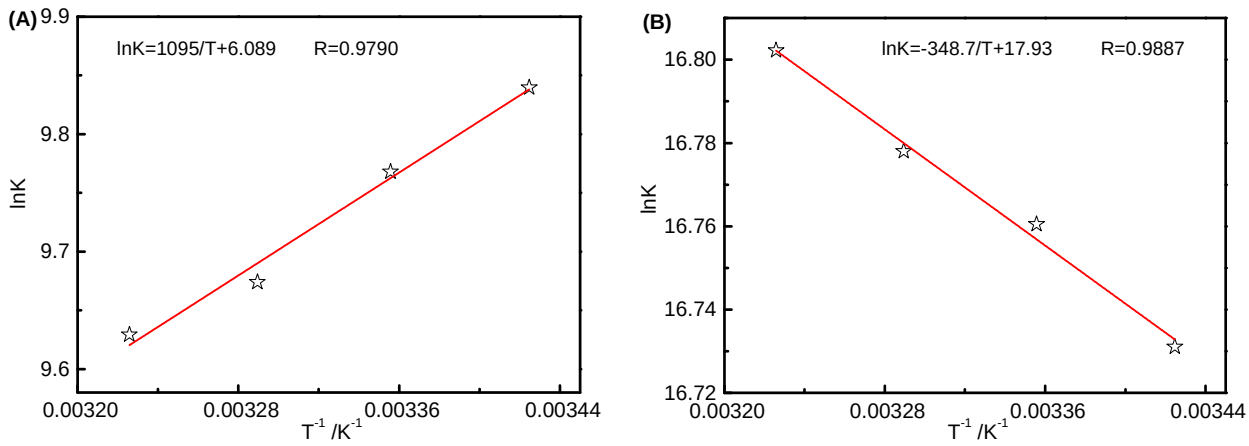

Fig. 7. The plots of logK versus 1/T for ABT-HSA (A) and MABT-HSA (B) interactions.

391

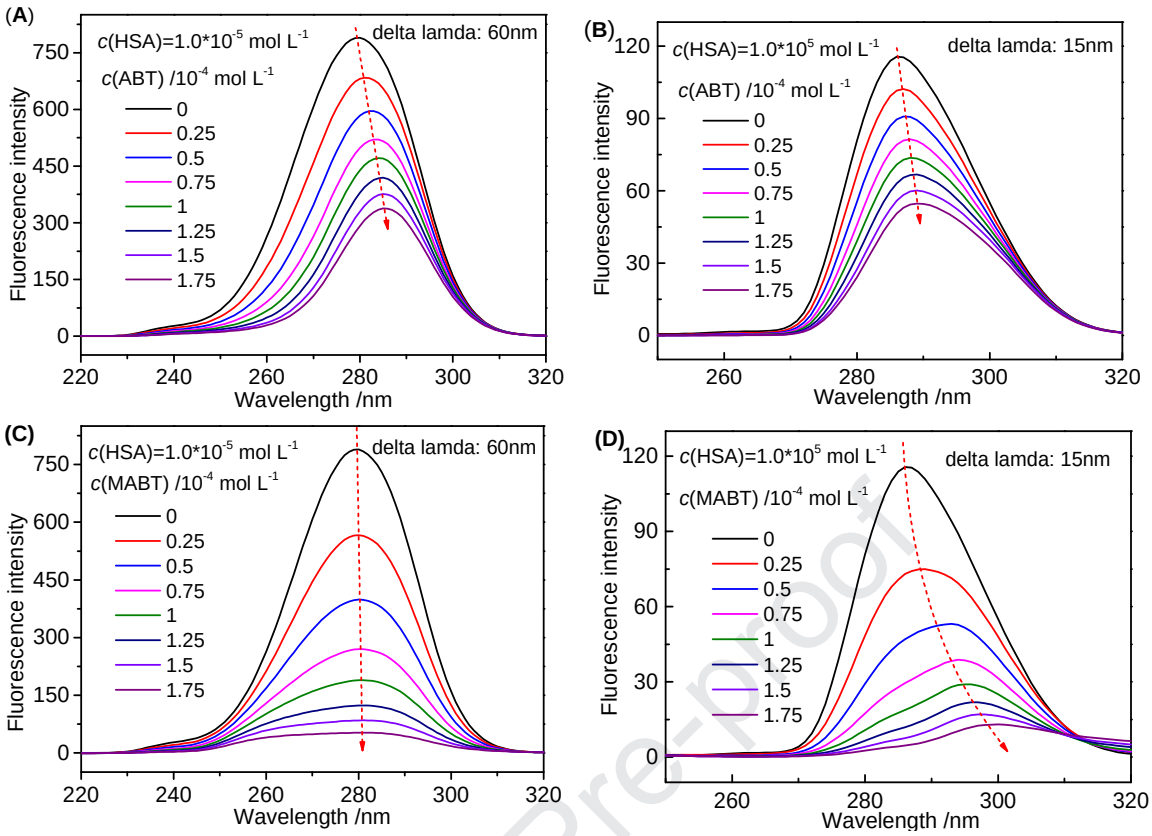

392

393 **Fig. 8.** SFE spectra of ABT-HSA and MABT-HSA systems.

394

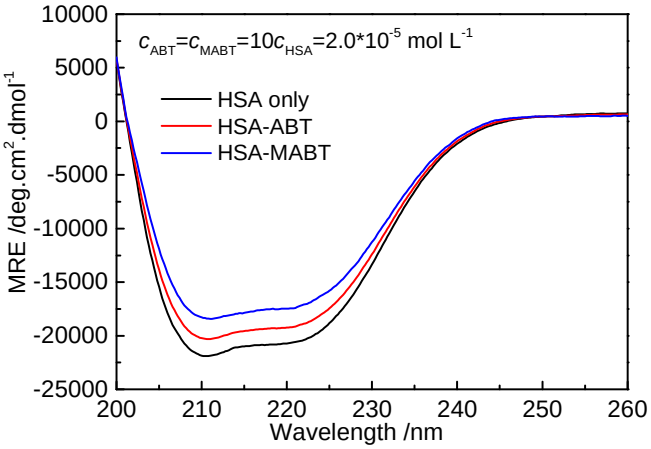

Fig. 9. Influence of ABT and MABT on CD spectra of HSA.

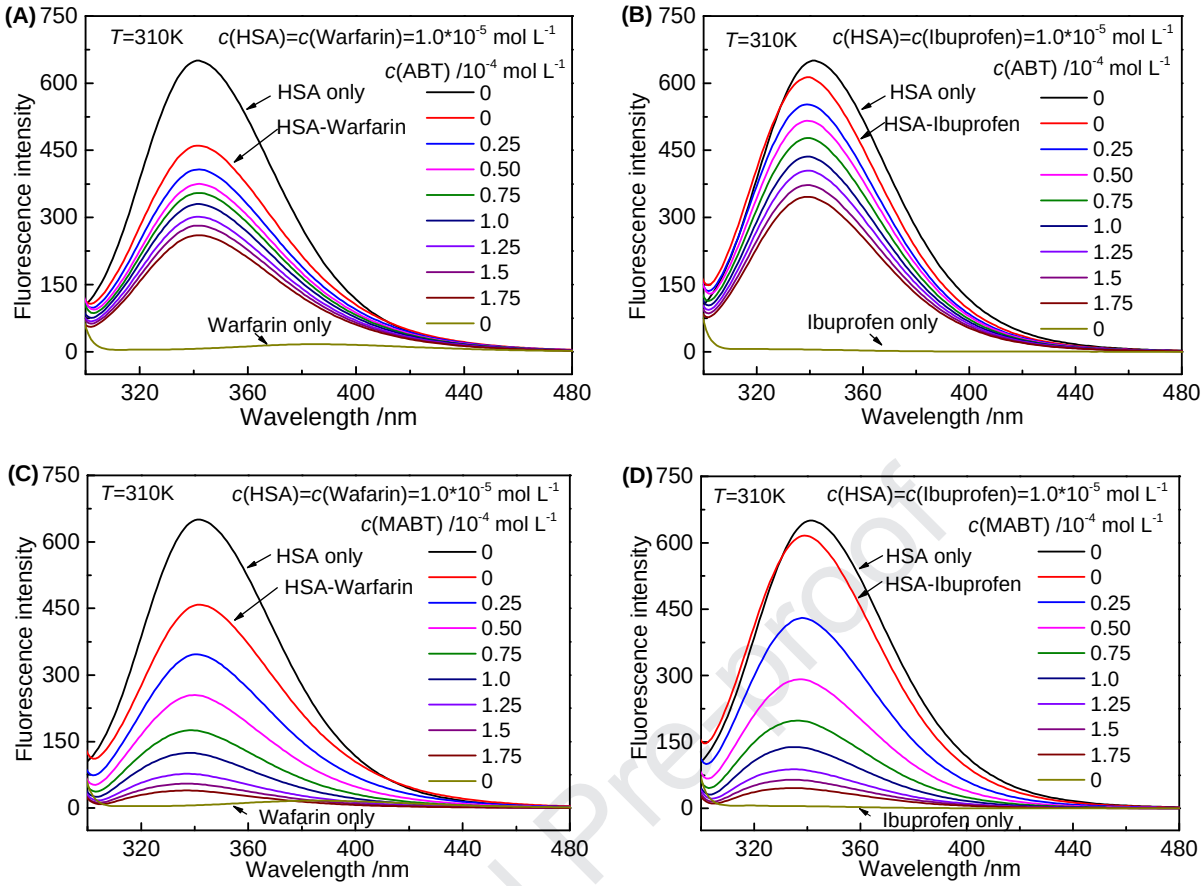

Fig. 10. Emission spectra of HSA-ABT and HSA-MABT systems after adding site markers.

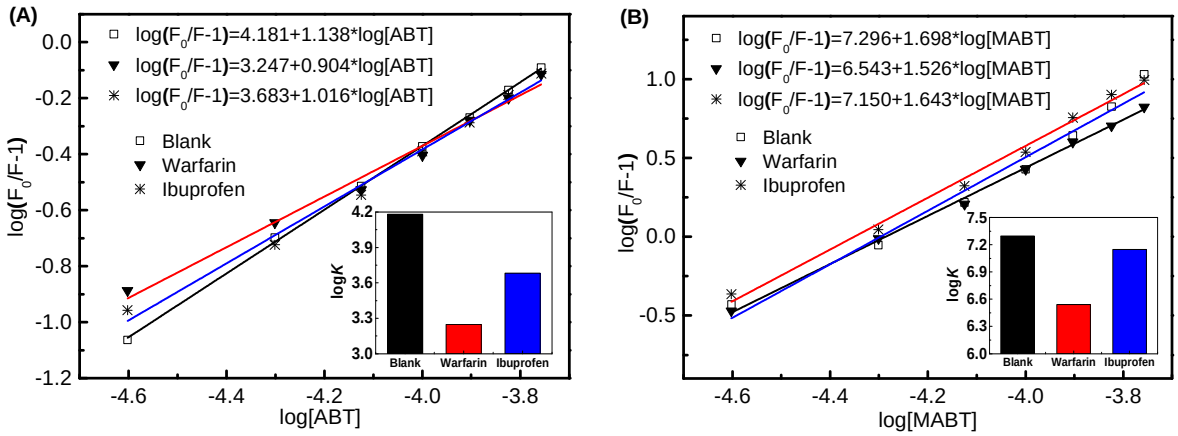

Fig. 11. Influence of probes on the equilibriums of HSA-ABT (A) and HSA-MABT (B) systems.

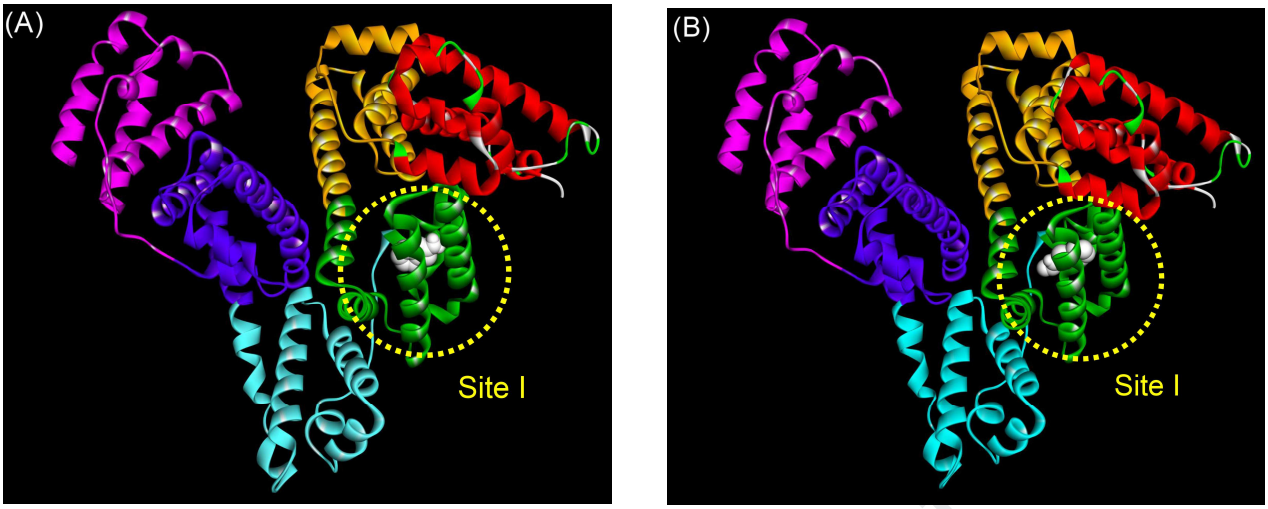

405

406 **Fig. 12.** The binding location of ABT (A) and MABT (B).

407

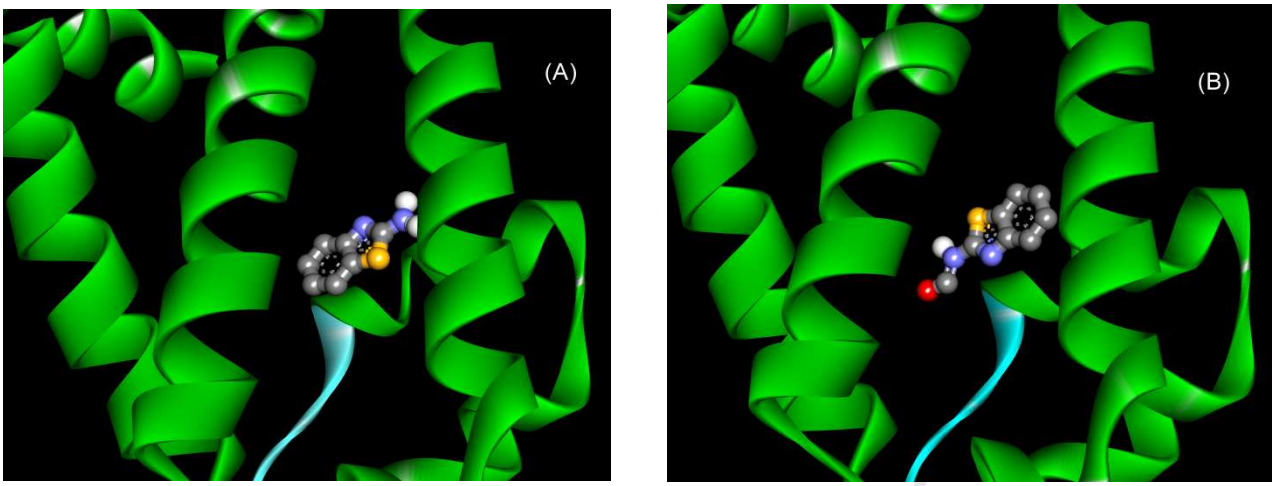

Fig. 13. The molecular orientation of ABT (A) and MABT (B) in new complexes.

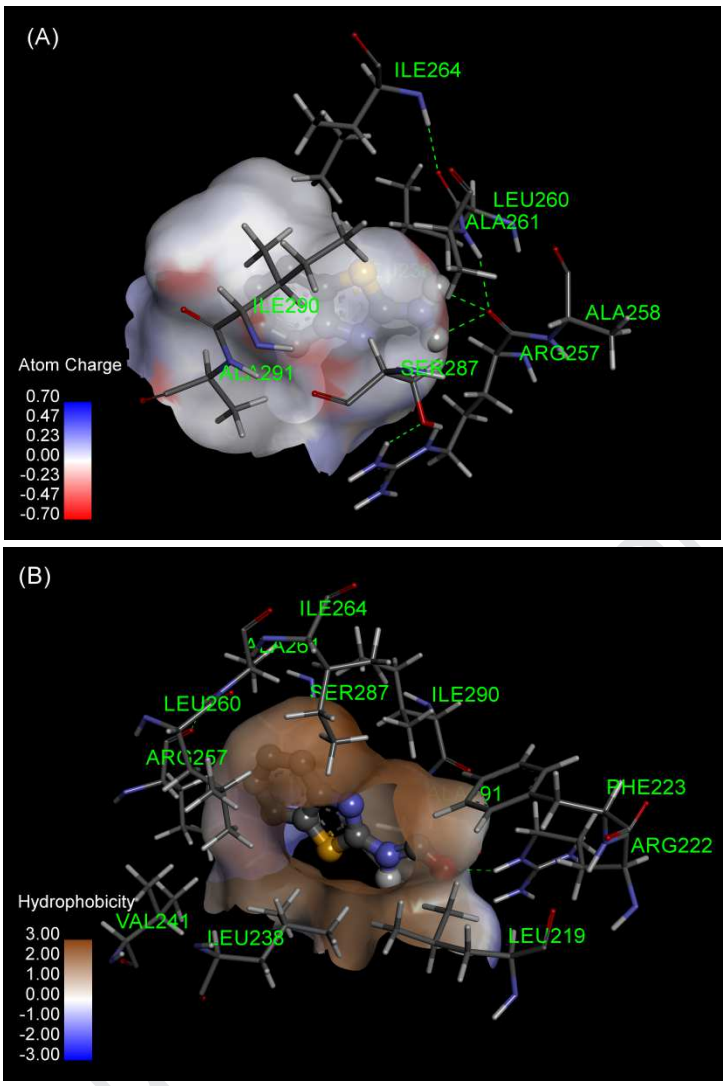

411

412

413 **Fig. 14.** Interaction of ABT (A) and MABT (B) with amino acid residues within 3.5Å.

414

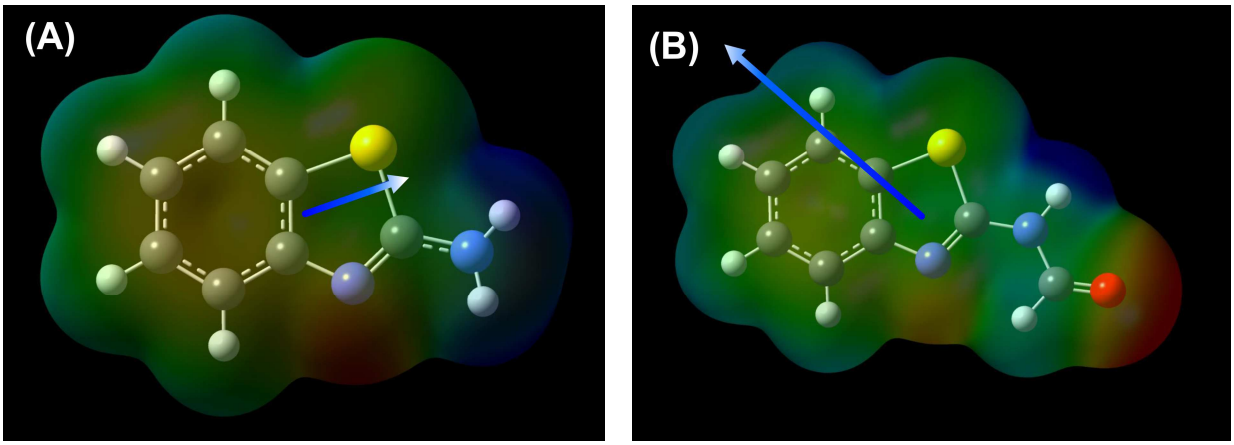

Fig. 15. The electrostatic potential and the dipole moments of ABT (A) and MABT (B).

Research Highlights

► MABT exhibited higher energy transfer efficiency and binding constants with HSA.

► The heterocyclic scaffold of benzothiazole and nitrogen atom guided ABT/MABT to Sudlow's site I.

► Their interactions with HSA were entropy-driven but with different heat effects.

► The opposite molecular orientations of ABT and MABT in new complex correlated with their directions of dipole moments.

► The energy gap between HOMO and LUMO of ligand molecules was responsible for their different energy transfer efficiency with HSA.